Simulation of non-vaporizing tubular nylon-6 reactors with radial gradients: finite-difference computations

Debasis Pal and Santosh K. Gupta*
Department of Chemical Engineering, Indian Institute of Technology, Kanpur 208016, India
(Received 4 March 1988; accepted 24 February 1989)

This work presents a comprehensive computer simulation study for the hydrolytic polymerization of ε-caprolactam without water removal in a continuous tubular reactor. It incorporates a laminar (Hagen–Poiseuille) or plug flow velocity profile, as well as radial thermal diffusion. The solution of the balance equations is carried out using two types of finite-difference techniques coupled with Gear's method for solving the ordinary differential equations so generated. Simulation results are obtained for various operating conditions. A comparison is made of the different methods used and their limitations are discussed. These results will form the basis for a comparison of the numerical results that could be generated using far more powerful computational tools like orthogonal collocation or finite-element techniques.

(Keywords: computer simulation; polymerization; ε-caprolactam; hydrolysis)

INTRODUCTION

The hydrolytic polymerization of ε-caprolactam is a very important commercial process and has drawn the attention of various researchers in recent years[1–16]. In fact, several excellent reviews[1–5] have appeared on this subject, emphasizing various aspects of the polymerization process.

The work on nylon-6 polymerization falls broadly into two categories. The emphasis in the early work was primarily on the determination of the polymerization mechanism and on the rate and equilibrium constants for the various reactions. These have been reviewed by Reimschuessel[1]. More recently, the emphasis has shifted to the study of physical processes like heat transfer, mass transfer, etc., associated with chemical reaction in large-scale reactors, and to the actual modelling and optimization of industrial reactors. Tai and Tagawa[2] and Kumar and Gupta[3,4] have reviewed these aspects.

The reaction mechanism comprises three major reactions, namely ring opening of caprolactam by water to form aminocaproic acid, and chain and step-growth reactions. In addition, there are several important side-reactions. Among these are the formation of cyclic oligomers, desamination and peroxidation of caprolactam[1]. The most important side-reactions are those associated with cyclic oligomers, since their presence in the product causes problems in its processing (e.g. in spinning and moulding). The kinetic scheme considered in this work is shown in *Table 1*. This includes the main reactions and the reactions associated with the cyclic dimer. The other cyclization reactions are omitted since their rate constants are not yet available. Moreover, it is well known[3,5] that the formation of the cyclic dimer predominates, and can be used as a first-order approximation of the total cyclics present.

The reactions are known to be catalysed by the carboxyl end-groups present in the reaction mass. The apparent rate constants are of the form

$$k_i = k_i^o + k_i^c[\text{–COOH}] \qquad (1)$$

with Arrhenius forms being used for k_i^o and k_i^c. All the reactions in *Table 1* are reversible in nature and the temperature dependences of the equilibrium constants are given by standard thermodynamic relations. The rate and equilibrium constants for the reactions of *Table 1* are given in *Table 2*. These are based on results from a series of experiments carried out by Tai *et al.*[6], using a non-linear regression analysis.

Various kinds of reactors, e.g. batch reactors, tubular reactors, continuous-flow stirred-tank reactors (CSTRs) and combinations thereof, are employed in industry to manufacture nylon-6. Computer simulations based on mathematical modelling of the polymerization processes in these reactors or their combinations offer information that is of paramount importance for quality control, process control and operational optimization of existing plant as well as in the design of new plant. Several studies have been reported on the simulation of both ideal reactors[7–9] and some common industrial reactors[10–13].

The present work focuses on the simulation of continuous tubular reactors with radial variations of temperature and concentrations accounted for. In most of the studies on tubular reactors reported up till now, radial variations of temperature (and hence of concentrations) have not been considered. This was probably to keep the analysis simple. The only study wherein such radial profiles are indeed computed is the one by Tai *et al.*[7], who study tubular reactors with heat removal by nitrogen stripping. These workers have used the two-dimensional (in the radial and axial directions) finite-difference computational technique to solve their balance equations after apparently (and erroneously) uncoupling the mass and energy balance equations. They

* To whom correspondence should be addressed

0032-3861/89/101918-13$03.00

have presented results on several other types of reactors and reactor combinations, and their work on tubular reactors is slightly less comprehensive than one would have liked. Our initial attempts on the optimization of such reactors has revealed the need for faster and more efficient computational techniques to integrate the modelling equations for such reactors, in order to cut down on the total computational costs. This work was undertaken to satisfy these needs, and presents detailed simulation results using two types of finite-difference algorithms. Results are generated for several conditions, e.g. for both plug and laminar flow velocity profiles in a tubular reactor and for both adiabatic and non-adiabatic operations. Results obtained with the two computational techniques and various model assumptions are compared. In addition to their intrinsic worth and interest, these results also form a reference with which results using more powerful and faster computational techniques (e.g. orthogonal collocation, orthogonal collocation on finite elements, etc., which could be used for optimization studies) can be compared in the future.

Table 1 Kinetic scheme for nylon-6 polymerization

1. Ring opening

$$C_1 + W \underset{k_1' = k_1/K_1}{\overset{k_1}{\rightleftharpoons}} P_1$$

2. Polycondensation

$$P_n + P_m \underset{k_2' = k_2/K_2}{\overset{k_2}{\rightleftharpoons}} P_{n+m} + W \qquad n, m = 1, 2, 3 \ldots$$

3. Polyaddition

$$P_n + C_1 \underset{k_3' = k_3/K_3}{\overset{k_3}{\rightleftharpoons}} P_{n+1} \qquad n = 1, 2, \ldots$$

4. Ring opening of cyclic dimer

$$C_2 + W \underset{k_4' = k_4/K_4}{\overset{k_4}{\rightleftharpoons}} P_2$$

5. Polyaddition of cyclic dimer

$$P_n + C_2 \underset{k_5' = k_5/K_5}{\overset{k_5}{\rightleftharpoons}} P_{n+2} \qquad n = 1, 2, \ldots$$

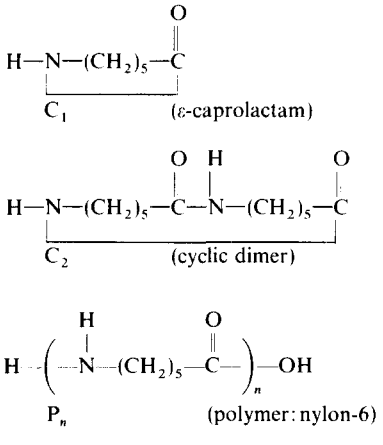

FORMULATION

Expressions for the rates of formation, R_ξ, of various species, ξ, in the reaction mixture and those of the first two moments[17–19], λ_0 and λ_1, defined by:

$$\lambda_k = \sum_{n=1}^{\infty} n^k [P_n] \qquad k = 0, 1, 2, \ldots \tag{2}$$

can easily be written from *Table 1*, and are available in our earlier work[5]. The heat generation rate ΔQ (kcal kg^{-1} h^{-1}) is expressed in terms of the net forward rates of the five reactions in *Table 1*, and is given in *Table 3*.

Table 4 shows the mass and heat balance equations as applied to a tubular reactor (see *Figure 1*) having a laminar (Hagen–Poiseuille) flow profile:

$$v_z = 2v_{av}(1 - r^2/R^2) \tag{3}$$

where v_{av} is the mean velocity (see 'Nomenclature' for definitions of terms). The average residence time, t, is given by:

$$t = z/v_{av} \tag{4}$$

where z is the distance along the reactor. In writing these equations, the diffusion of all the components has been neglected and only thermal diffusion in the radial direction has been considered. Whereas the diffusion of heavy polymer molecules may indeed be negligible, it may not be quite justified to neglect the diffusion of the lower-molecular-weight components, particularly monomer and water. This assumption is made for two

Table 3 Rate of heat generation:

$$\Delta Q = \sum_{i=1}^{5} (-\Delta H)_i R_i / 10^3$$

$$R_1 = k_1[C_1][W] - k_1'[P_1] \tag{a}$$

$$R_2 = k_2\lambda_0^2 - k_2'[W](\lambda_1 - \lambda_0) \tag{b}$$

$$R_3 = k_3[C_1]\lambda_0 - k_3'(\lambda_0 - [P_1]) \tag{c}$$

$$R_4 = k_4[C_2][W] - k_4'[P_2] \tag{d}$$

$$R_5 = k_5[C_2]\lambda_0 - k_5'(\lambda_0 - [P_1] - [P_2]) \tag{e}$$

Table 2 Rate and equilibrium constants for nylon-6 polymerization[2]:

$k_i = k_i^a + k_i^c[-COOH] = A_i^a \exp(-E_i^a/R_gT) + A_i^c \exp(-E_i^c/R_gT)[-COOH]$

$K_i = \exp(\Delta S_i/R_g - \Delta H_i/R_gT) \qquad i = 1, 2, \ldots, 5$

i	A_i^a (kg mol^{-1} h^{-1})	E_i^a (cal mol^{-1})	A_i^c (kg^2 mol^{-2} h^{-1})	E_i^c (cal mol^{-1})	ΔH_i (cal mol^{-1})	ΔS_i (eu)
1	5.9874×10^5	1.9880×10^4	4.3075×10^7	1.8806×10^4	1.9180×10^3	-7.8846
2	1.8942×10^{10}	2.3271×10^4	1.2114×10^{10}	2.0670×10^4	-5.9458×10^3	9.4374×10^{-1}
3	2.8558×10^9	2.2845×10^4	1.6377×10^{10}	2.0107×10^4	-4.0438×10^3	-6.9457
4	8.5778×10^{11}	4.2000×10^4	2.3307×10^{12}	3.7400×10^4	-9.6000×10^3	-1.4520×10^1
5	2.5701×10^8	2.1300×10^4	3.0110×10^9	2.0400×10^4	-3.1691×10^3	5.8265×10^{-1}

Table 4 Mass and heat balance equations in a tubular reactor with laminar flow profile[a]

Mass balance

$$2(1-r^2/R^2)\mathrm{d}[C_1]/\mathrm{d}t = R_{C_1} \quad \text{(a)}$$

$$2(1-r^2/R^2)\mathrm{d}[P_1]/\mathrm{d}t = R_{P_1} \quad \text{(b)}$$

$$2(1-r^2/R^2)\mathrm{d}\lambda_0/\mathrm{d}t = R_{\lambda_0} \quad \text{(c)}$$

$$2(1-r^2/R^2)\mathrm{d}\lambda_1/\mathrm{d}t = R_{\lambda_1} \quad \text{(d)}$$

$$2(1-r^2/R^2)\mathrm{d}[C_2]/\mathrm{d}t = R_{C_2} \quad \text{(e)}$$

$$2(1-r^2/R^2)\mathrm{d}[W]/\mathrm{d}t = R_W \quad \text{(f)}$$

Heat balance

$$2(1-r^2/R^2)\rho C_P \frac{\partial T}{\partial t} = \frac{k\partial}{r\partial r}\left(r\frac{\partial T}{\partial r}\right) + \rho(\Delta Q) \quad \text{(g)}$$

Boundary conditions

$$-k\left(\frac{\partial T}{\partial r}\right)_{r=R} = h(T-T_j) \quad \text{(h)}$$

$$\left(\frac{\partial T}{\partial r}\right)_{r=0} = 0 \quad \text{(i)}$$

[a] See 'Nomenclature'; R_ξ available in ref. 5

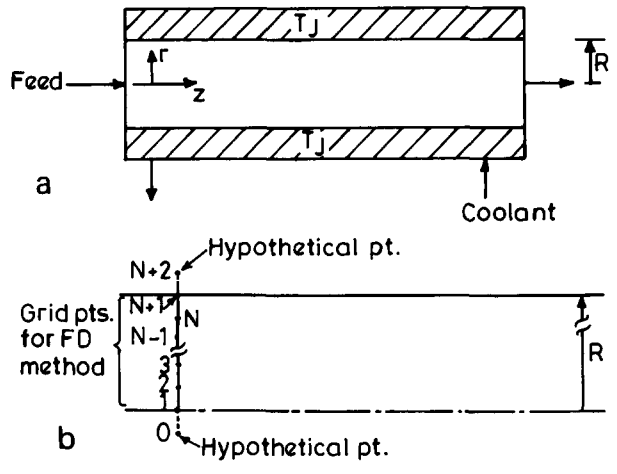

Figure 1 (a) Schematic representation of the tubular reactor with cooling jacket. (b) Grid points for the finite-difference technique (methods I and II)

reasons—first, because precise data on the diffusion coefficients are still not available[14], and secondly, since radial diffusion in the absence of vaporization is expected to be a second-order effect. Tai *et al.*[7] have also made similar approximations. It may be pointed out here that some work has been reported recently by Hamer and Ray[20] on the detailed modelling of continuous tubular chain polymerization reactors incorporating radial mass diffusion as well as accounting for property and velocity variations. Work along these lines for nylon-6 reactors could be carried out, but since our long-range focus was on optimization studies, we did not pursue this approach.

The following correlations[7,21] have been used for the various thermophysical properties:

thermal conductivity

$$k = 0.21 \text{ kcal m}^{-1}\text{K}^{-1}\text{h}^{-1} \quad \text{(5a)}$$

density

$$\rho(\text{kg m}^{-3}) = 1000\{1.0065 + 0.0123[C_1] + [T(\text{K}) - 495](0.00035 + 0.00007[C_1]\}^{-1} \quad \text{(5b)}$$

specific heat

$$C_P(\text{kcal kg}^{-1}\text{K}^{-1}) = 0.6593[C_1]/[C_1]_0 + (1-[C_1]/[C_1]_0)[0.4861 + 0.000337T(\text{K})] \quad \text{(5c)}$$

The boundary condition at the wall of the reactor for the heat balance equation (equation (h) in *Table 4*) is obtained by considering a coolant at a constant temperature, T_j (K), circulated in a jacket enclosing the reactor (*Figure 1a*), with the overall heat transfer coefficient h. The symmetry condition at $r=0$ is given by equation (i) in *Table 4*.

A radial temperature gradient will be established in the reactor at any cross-section along the length because of the presence of the velocity profile as well as due to the heat flux through the wall. As a consequence, the concentrations of all the species will also have a radial variation. Hence, the variables $[C_1]$, $[P_1]$, λ_0, λ_1, $[C_2]$, $[W]$ and T are all functions of r and t in general, and can be represented as $[C_1](r, t)$, etc. To obtain all these profiles, the set of partial differential equations (PDEs) (equations (a)–(g) in *Table 4*) need to be integrated simultaneously with the boundary and symmetry conditions (equations (h)–(i) in *Table 4*). In addition, the closure approximation:

$$[P_3] = [P_2] = [P_1] \quad (6)$$

is employed. This was first used by Reimschuessel[1]. Tai *et al.*[22] have found that the final results are insensitive to this assumption under various conditions.

To use the finite-difference (FD)[23] method, the radial distance, $\phi \leqslant r \leqslant R$, is first divided into N equal parts, each of length Δr, using $(N+1)$ grid points numbered from 1 to $N+1$ (*Figure 1b*). Thus, the jth radial grid point at $r = r_j$ is at $r = (j-1)(\Delta r)$. The variables at r_j are renamed for the sake of convenience as follows:

$$U_{i,j}(t) \equiv \xi_i(r_j, t) \qquad i = 1, 2, \ldots, 7 \quad (7a)$$

$$j = 1, 2, \ldots, N+1$$

$$\xi \equiv [[C_1], [P_1], \lambda_0, \lambda_1, [C_2], [W], T] \quad (7b)$$

The radial derivatives (equation (g) in *Table 4*), the boundary condition (equation (h) in *Table 4*) and the symmetry condition (equation (i) in *Table 4*) are converted into algebraic expressions using the FD technique[23]. This has been done in two different ways. In the first method (method I), the Laplacian in the heat balance (equation (g) in *Table 4*) is broken up into two parts to give:

$$2(1-r^2/R^2)\rho C_P \frac{\partial T}{\partial t} = \frac{k}{r}\frac{\partial T}{\partial r} + k\frac{\partial^2 T}{\partial r^2} + \rho(\Delta Q) \quad (8)$$

The finite-difference formulae[23] for the first and second derivatives (mid-point formulae) are then applied to give the following ordinary differential equation (ODE) corresponding to the jth point:

$$2(1-r_j^2/R^2)\rho_j(C_P)_j \frac{\mathrm{d}U_{7,j}}{\mathrm{d}t} = k\left(\frac{1}{r_j}\frac{U_{7,j+1}-U_{7,j-1}}{2(\Delta r)} + \frac{U_{7,j+1}-2U_{7,j}+U_{7,j-1}}{(\Delta r)^2}\right) + \rho_j(\Delta Q)_j \qquad j = 2, \ldots, N \quad (9)$$

At the centre, i.e. at $j=1$ ($r=0$), equation (9) presents a

problem, because it involves U_7 at an undefined point, $j=0$, as well as division by zero (since $r_1=0$). This is resolved by using L'Hospital's rule as well as the symmetry condition in its FD form[23]:

$$\frac{U_{7,2}-U_{7,0}}{2(\Delta r)}=0 \quad \text{or} \quad U_{7,0}=U_{7,2} \tag{10}$$

Here, $U_{7,0}$ is the temperature at a hypothetical point, $j=0$ (*Figure 1b*). The resulting equation corresponding to $j=1$ is:

$$2(1-r_1^2/R^2)\rho_1(C_p)_1\,dU_{7,1}/dt = [4k/(\Delta r)^2](U_{7,2}-U_{7,1})+\rho_1(\Delta Q)_1 \tag{11}$$

Similarly equation (9) for $j=N+1$ ($r=R$, at the wall) involves $U_{7,N+2}$, the temperature at another hypothetical point. This is resolved by using the FD form of the boundary condition (equation (h) in *Table 4*):

$$U_{7,N+2}=U_{7,N}-[2(\Delta r)h/k](U_{7,N+1}-T_j) \tag{12}$$

This is used in equation (9) for $j=N+1$. The set of mass balance equations can be transformed to the FD form quite easily. Thus, $7(N+1)$ ordinary differential equations have been generated, which are given in *Table 5*. The number of variables to be solved for is also $7(N+1)$. These ODEs are solved using Gear's package[23], which has a built-in step size control algorithm and is particularly useful for stiff systems. The NAG Library Routine DO2EBF was used for this purpose in a DEC 1090 system.

The second approach of the finite-difference technique (method II) is very similar to method I except at the boundary points, $j=1$ and $N+1$. To apply the FD technique to the boundary and the symmetry condition, the one-sided first derivative formulae (ref. 12, p. 68), which have the same degree of accuracy as the mid-point formulae used in method I, have to be used. The symmetry condition at $r=0$ is transformed into:

$$U_{7,1}=\frac{4}{3}U_{7,2}-\frac{1}{3}U_{7,3} \tag{13}$$

and the boundary condition at $r=R$ gives:

$$U_{7,N+1}=\frac{hT_j-[k/2(\Delta r)](U_{7,N-1}-4U_{7,N})}{h+[3k/2(\Delta r)]} \tag{14}$$

Table 5 Set of differential equations after applying method I of finite-difference technique[a]

$$2(1-r_j^2/R^2)\,dU_{1,j}/dt=(R_{U_1})_j \quad j=1,\ldots,N+1 \tag{a}$$

$$2(1-r_j^2/R^2)\,dU_{2,j}/dt=(R_{U_2})_j \quad j=1,\ldots,N+1 \tag{b}$$

$$2(1-r_j^2/R^2)\,dU_{6,j}/dt=(R_{U_6})_j \quad j=1,\ldots,N+1 \tag{c}$$

$$2(1-r_1^2/R^2)\rho_1(C_p)_1\frac{dU_{7,1}}{dt}=\frac{4k}{(\Delta r)^2}(U_{7,2}-U_{7,1})+\rho_1(\Delta Q)_1 \tag{d}$$

$$2(1-r_j^2/R^2)\rho_j(C_p)_j\frac{dU_{7,1}}{dt} = k\left(\frac{1}{r_j}\frac{U_{7,j+1}-U_{7,j-1}}{2(\Delta r)}+\frac{U_{7,j+1}-2U_{7,j}+U_{7,j-1}}{(\Delta r)^2}\right) + \rho_j(\Delta Q)_j \quad j=2,\ldots,N+1 \tag{e}$$

with

$$U_{7,N+2}=U_{7,N}-[2(\Delta r)h/k](U_{7,N+1}-T_j)$$

[a] Dependence of variables on t is not explicitly mentioned

The FD form of the heat balance equation (similar to equation (9) at the centre and boundary points is thus avoided by using equations (13) and (14). This could be interpreted to mean that one is neglecting heat generation effects near the central and wall grid points. The resultant set of ODEs consists of equations (a)–(c) in *Table 5* for $j=1,\ldots,N+1$ and equation (e) in *Table 5* for $j=2,\ldots,N$. The total number of ODEs is $7(N+1)-2$ and the number of variables is also $7(N+1)-2$. The other two variables, i.e. the temperatures at the centre and at the external boundary point, can be obtained from equations (13) and (14). The same Gear's package is used for integrating the set of equations as in method I.

A compact computer package for integrating the PDEs (NAG Library Routine D03PBF) was also used (method III). This package consists of a combination of the finite-difference technique and Gear's package to solve a set of PDEs with appropriate boundary conditions. As discussed later, methods I and III are essentially the same. However, method III has an additional flexibility in the sense that it can be used for any type of unequal grid spacing, upon changing an input integer, IMESH. The value used for our case was IMESH = 4, which results in having more grid points near the external boundary (where the gradients are expected to be steeper) according to the formula:

$$r_i=R\sin[\pi(i-1)/2N] \quad i=1,2,\ldots,N+1 \tag{15}$$

This method was used to generate various simulation results.

In all the numerical techniques, the variables obtained at the radial grid points at any t are used to get the average values. The averages can be computed using the 'cup mixing rule' to give, for any concentration and moment:

$$\bar{U}_i(t)=\frac{\int_0^R r(1-r^2/R^2)U_i(r,t)\rho(r)\,dr}{\int_0^R r(1-r^2/R^2)\rho(r)\,dr} \quad \text{for } i=1,\ldots,6 \tag{16}$$

and for temperature:

$$\bar{U}_7(t)=\frac{\int_0^R r(1-r^2/R^2)U_7(r,t)\rho(r)C_p(r)\,dr}{\int_0^R r(1-r^2/R^2)\rho(r)C_p(r)\,dr} \tag{17}$$

The integrals are computed by employing a third-order finite-difference formula given by Gill and Miller[24]. The NAG Library Routine D01GAF is used for this purpose.

In true laminar flow, the residence time at the wall is infinity. To avoid numerical problems, a small slip ($v_z(R)/v_{av}=10^{-4}$) was assumed at the wall. The numerical results were found to be relatively unaffected by changing the dimensionless velocity around 10^{-4}. The inlet condition at the point $r=R$, $t=0$, was also modified. The equilibrium conversion values of isothermal runs at 250°C were fed in as values at $r=R$, $t=0$. This reduced the computational time significantly and avoided convergence problems. Any change in these input values was found not to affect the results, but led to longer computational times.

RESULTS AND DISCUSSION

A general computer program was made. Results for isothermal conditions could be obtained by putting $Q=0$ in the computer program. Similarly, adiabatic operation could be simulated by putting the overall heat transfer coefficient, $h=0$. The program could be run using either plug flow (v_z = constant = v_{av}) or parabolic flow (equation (3)) profiles. A typical run for $t=20$ h and 10 FD points took 3 min 45 s on a DEC 1090 system.

The computer programs for all three methods described previously were checked with results available in the literature[10,25]. The programs were run for the simple case of an isothermal plug flow reactor with the input variables:

$$\begin{aligned} [C_1]_0 &= 8.8\ \text{mol kg}^{-1} \\ [W]_0 &= 0.16\ \text{mol kg}^{-1} \\ [P_1]_0 &= (\lambda_0)_0 = (\lambda_1)_0 = [C_2]_0 = 0 \\ R &= 0.6\ \text{m} \end{aligned} \tag{18}$$

and for temperatures of 230, 240, 250 and 270°C. The results were found to be in complete agreement with those of Ray and Gupta[25], thus confirming the correctness of the computer programs (except the heat balance equation, which is not required for the isothermal reactor). The programs were also run for an adiabatic plug flow reactor with the feed coming from the top of a VK column[10]. The results were found to match those of Gupta and Gandhi[10]. This further confirmed the correctness of our computer programs (including the heat balance equation).

Having developed confidence in the computer packages prepared, detailed temperature and concentration profiles for several conditions were generated. The feed conditions were the same as in equation (18). *Table 6* gives the various flow and heat transfer conditions used. *Figures 2* and *17* present profiles for monomer conversion, number-average chain length ($\mu_n=\lambda_1/\lambda_0$), temperature and cyclic dimer concentration for various values of t ($\equiv z/v_{av}$). For heat transfer coefficient, h, a typical value[11] of 5.0 kcal m^{-2} h^{-1} was used. The existence of distinct concentration and temperature profiles is quite evident from these figures. These profiles can be obtained from any of the three FD algorithms, using a sufficiently large number of grid points.

Figures 2 and *5* show the profiles at $t=5$ h for various flow and heat transfer conditions (*Table 6*). The laminar flow case (curves 4, 5 and 6) is the most interesting. Since the velocity near the centre is higher, the residence time of a fluid element near the wall (at the same t) is far larger when compared to that of a fluid element near the centre. Thus, the reaction is close to equilibrium at the wall. A maximum in the temperature slightly away from the wall is observed (curves 5 and 6 in *Figure 2*) at $t=5$ h. This represents a combination of higher heat generation (due to higher near-equilibrium conversion) near the wall as well as heat transfer effects. In the laminar adiabatic case (curve 5 in *Figure 2*), a temperature maximum first appears (at t near zero) at the wall because of almost instantaneous attainment of equilibrium conversions there. The high temperature leads to thermal diffusion away from the wall as t increases (since $h=0$), contributing to a decrease in the temperature at the wall. In addition, as t increases, layers adjacent to the wall reach near-equilibrium conversion (curves 5 and 6 in *Figures 3* to *5*), generating more heat there. This explains the temperature maximum in curve 5 of *Figure 2*. The peak shifts further inwards as t increases (*Figure 6*). Because of cooling from the jacket, the temperatures at the wall are lower for the laminar non-adiabatic case (curve 6 of *Figure 2*). The slightly higher near-equilibrium

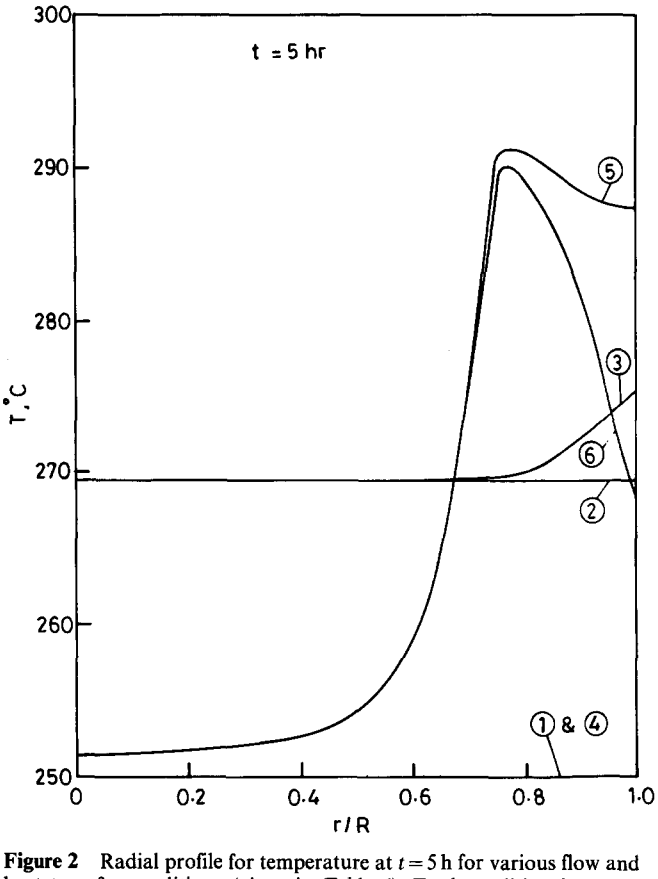

Figure 2 Radial profile for temperature at $t=5$ h for various flow and heat transfer conditions (given in *Table 6*). Feed condition is as per equation (18)

Table 6 Various flow and heat transfer conditions used in simulation runs

Run no.	Type of flow	Heat transfer condition	Heat transfer coefficient, h(kcal m^{-2} K^{-1} h^{-1})	Feed temp., T_0 (°C)	Coolant temp., T_j (°C)
1	Plug	Isothermal	–	250	–
2	Plug	Adiabatic	0	250	–
3	Plug	Non-adiabatic	5.0	250	260
4	Laminar	Isothermal	–	250	–
5	Laminar	Adiabatic	0	250	–
6	Laminar	Non-adiabatic	5.0	250	260

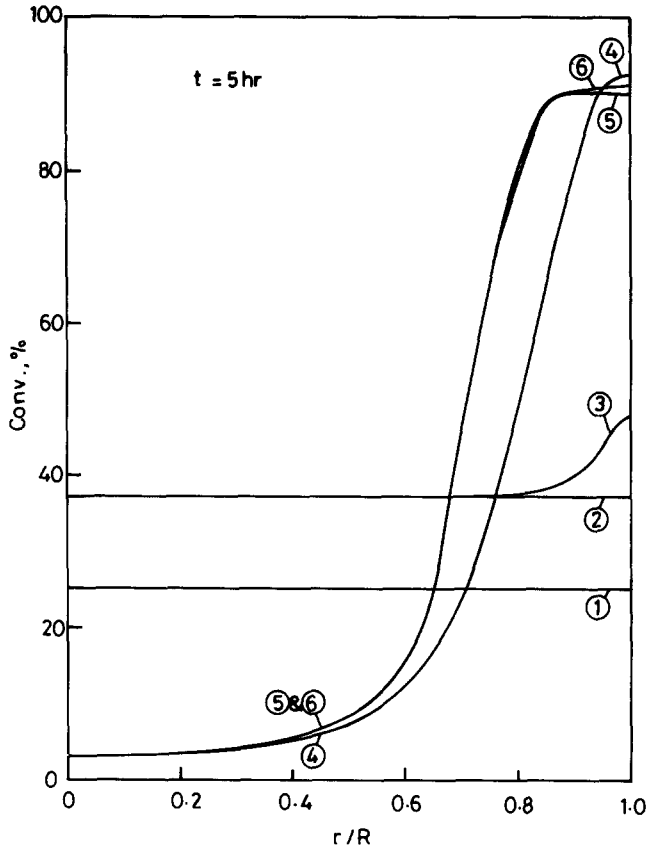

Figure 3 Radial profile for monomer conversion at $t = 5$ h. Conditions as in *Figure 2*

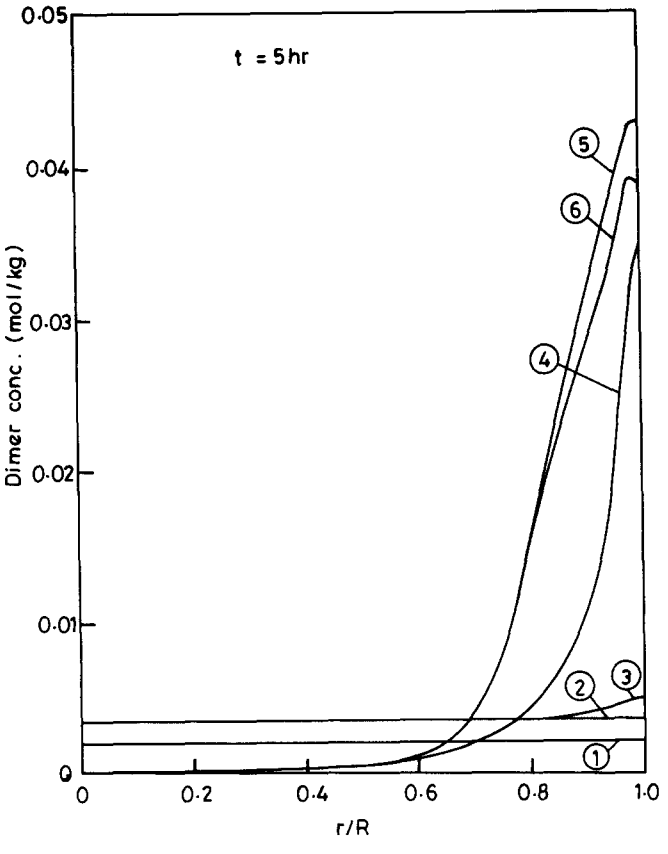

Figure 5 Radial profile for $[C_2]$ at $t = 5$ h. Conditions as in *Figure 2*

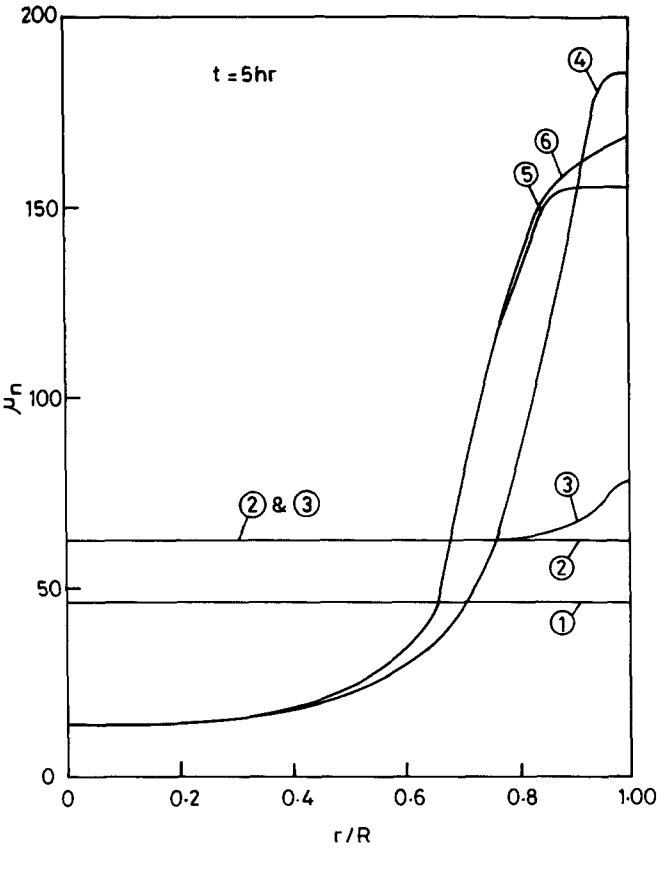

Figure 4 Radial profile for μ_n at $t = 5$ h. Conditions as in *Figure 2*

conversion for curve 6 in *Figure 2* (compared to curve 5) is because of the lower temperatures present and the overall exothermic nature of the reactions. Since the equilibrium values of μ_n are more sensitive to temperature, the difference between curves 5 and 6 in *Figure 4* is greater. In plug flow, the residence times of fluid elements at the wall are not infinite, and so near-equilibrium conditions do not prevail at the wall for this ideal reactor. In the adiabatic case, the temperature (and other) profiles are flat, as expected, since there is no driving force for creating radial differences. For the plug flow non-adiabatic case (curve 3 in *Figure 2*) a temperature maximum near the wall develops again. Near $t = 0$, a maximum appears at the wall ($T_J > T_0$). This leads to higher conversions at the wall, which simultaneously leads to higher heat generation by reaction at that point. Very soon the temperature at the wall increases beyond T_J. Heat transfer takes place both to the jacket as well as towards the centre. The conversion is the highest at the wall for case 3 (*Figure 3*) since it represents a cumulative effect from $t = 0$ to 5. *Figures 6* to *17* show conditions at $t = 10$, 15 and 20 h. The trends at $t = 5$ h continue, but some flattening of temperature profiles is observed, because of thermal diffusion effects away from the peak, both towards the wall as well as towards the centre. The conversion, μ_n, and cyclic dimer concentration profiles show higher levels near the centre as t increases, as expected. *Figures 15* and *17*, at $t = 20$ h, show that even though the monomer conversion has almost attained equilibrium values throughout the cross-section, lower cyclic dimer concentrations near the centre are observed.

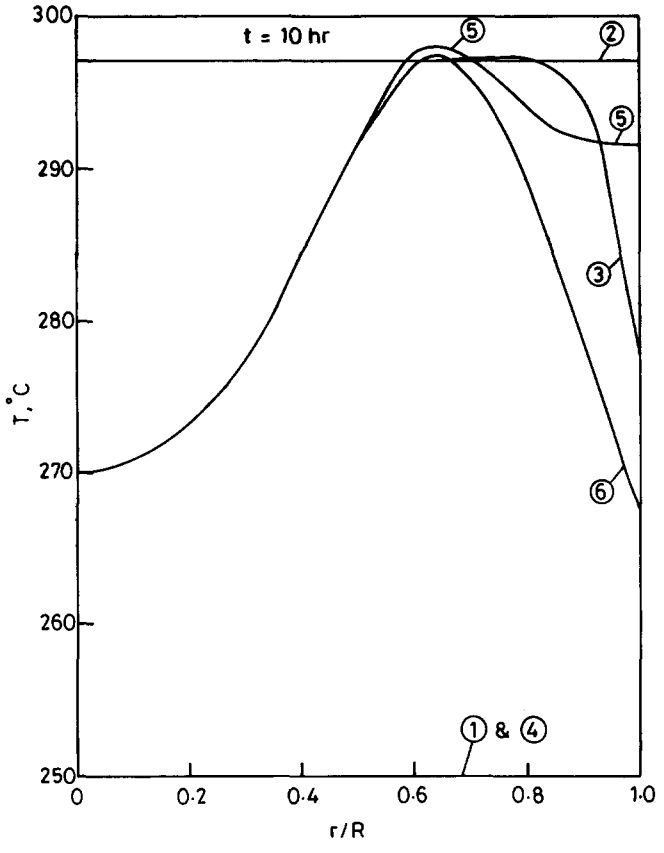

Figure 6 Radial profile for temperature at $t = 10$ h for various flow and heat transfer conditions (given in *Table 6*). Feed condition is as per equation (18)

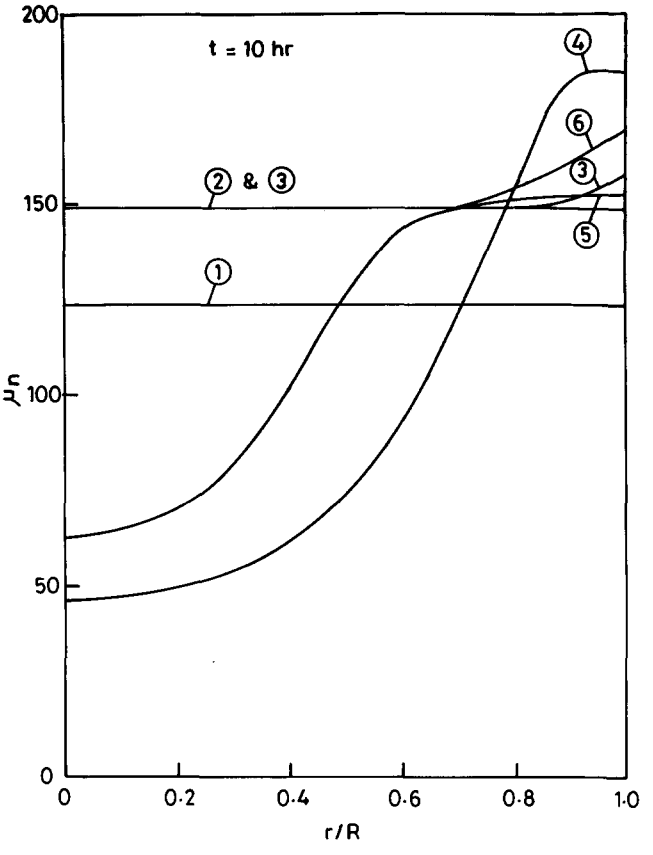

Figure 8 Radial profile for μ_n at $t = 10$ h. Conditions as in *Figure 6*

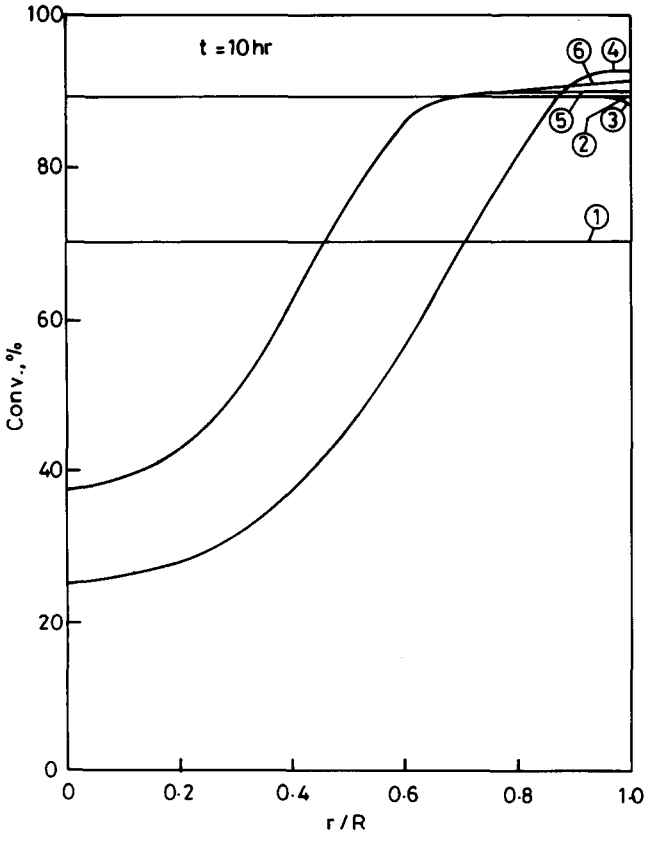

Figure 7 Radial profile for conversion at $t = 10$ h. Conditions as in *Figure 6*

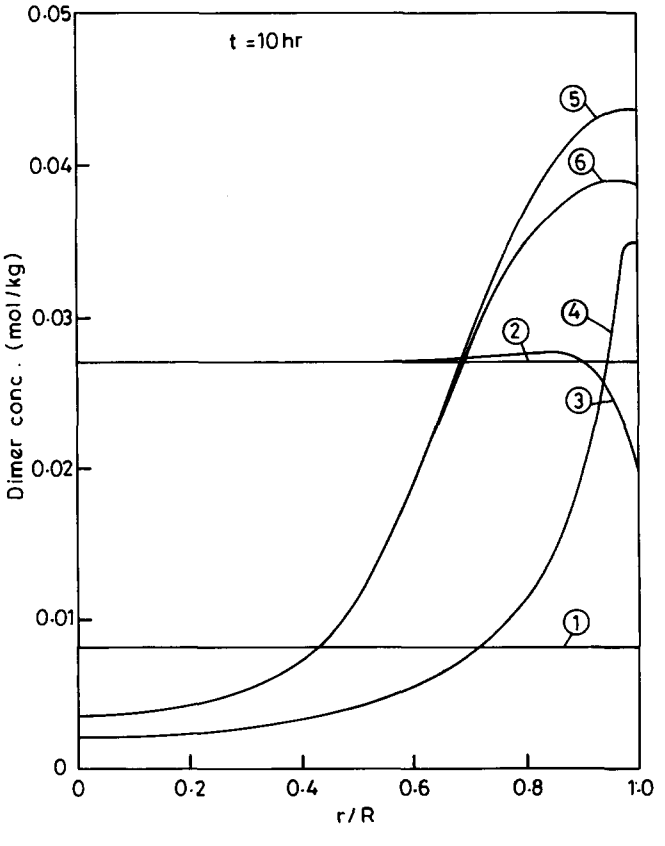

Figure 9 Radial profile $[C_2]$ at $t = 10$ h. Conditions as in *Figure 6*

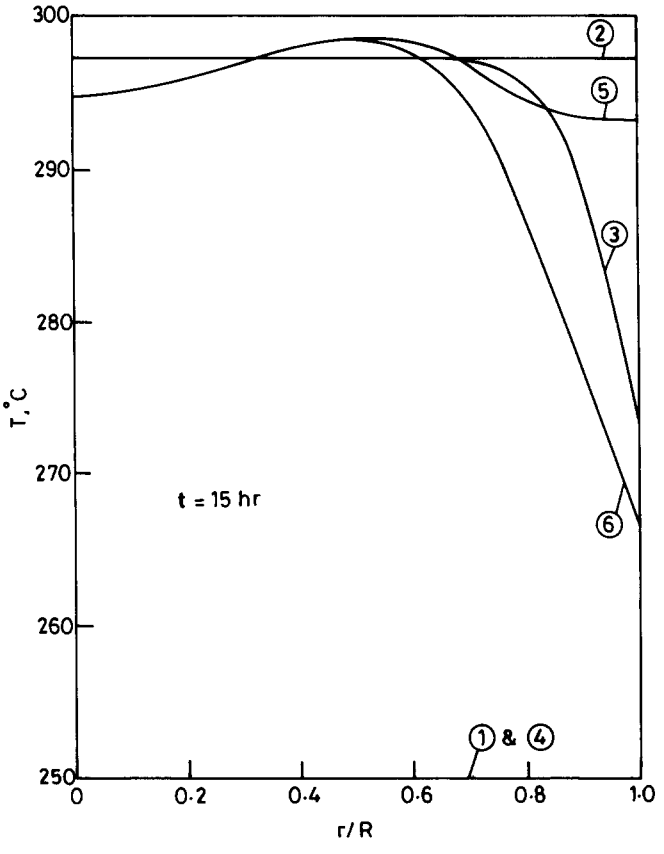

Figure 10 Radial profile for temperature at $t = 15$ h for various flow and heat transfer conditions (given in *Table 6*). Feed condition is as per equation (18)

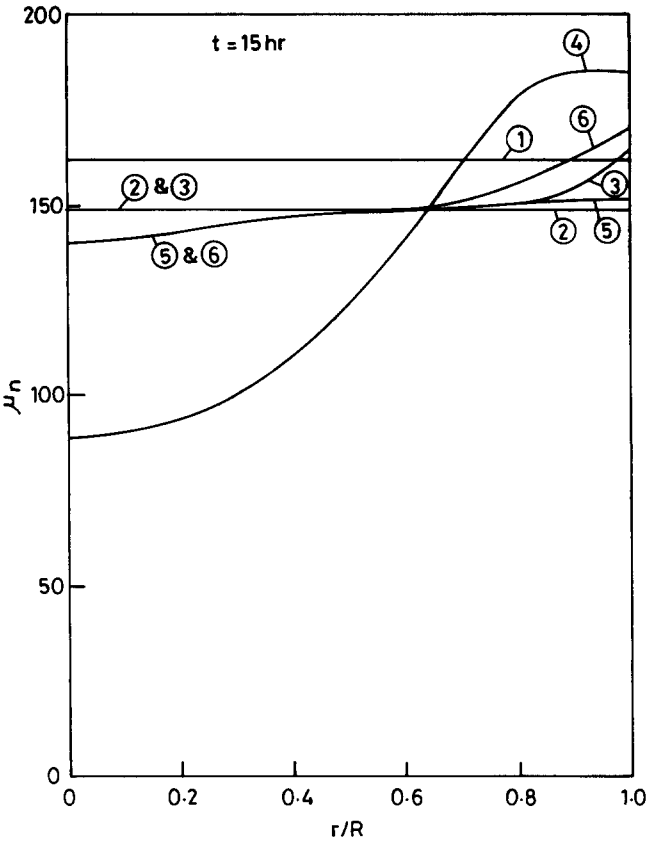

Figure 12 Radial profile for μ_n at $t = 15$ h. Conditions as in *Figure 10*

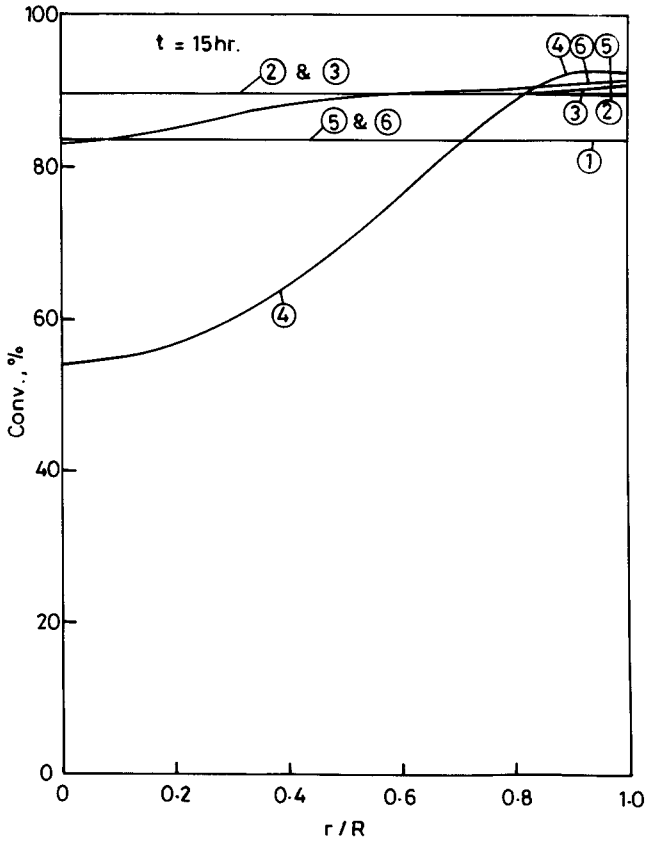

Figure 11 Radial profile for conversion at $t = 15$ h. Conditions as in *Figure 10*

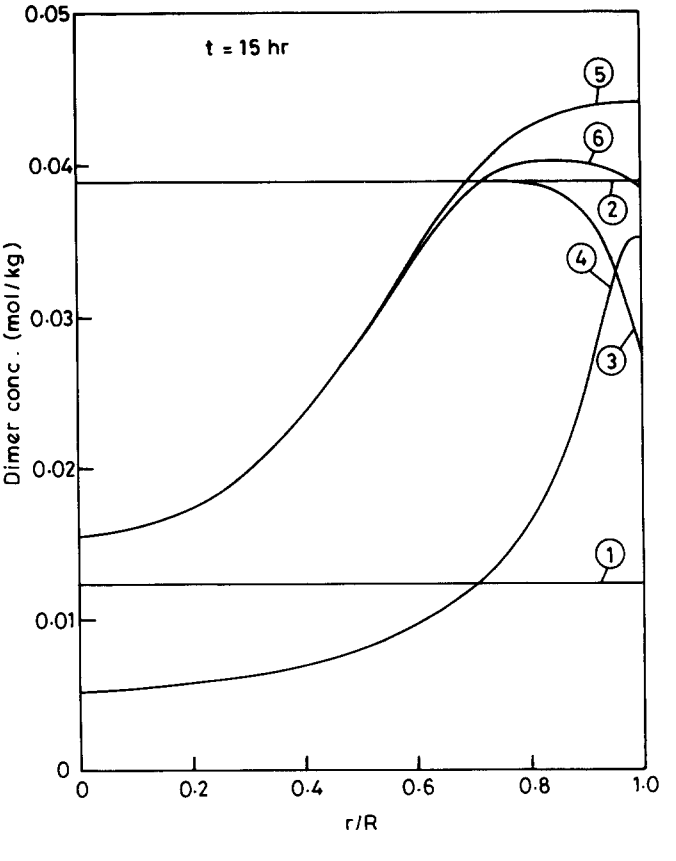

Figure 13 Radial profile for $[C_2]$ at $t = 15$ h. Conditions as in *Figure 10*

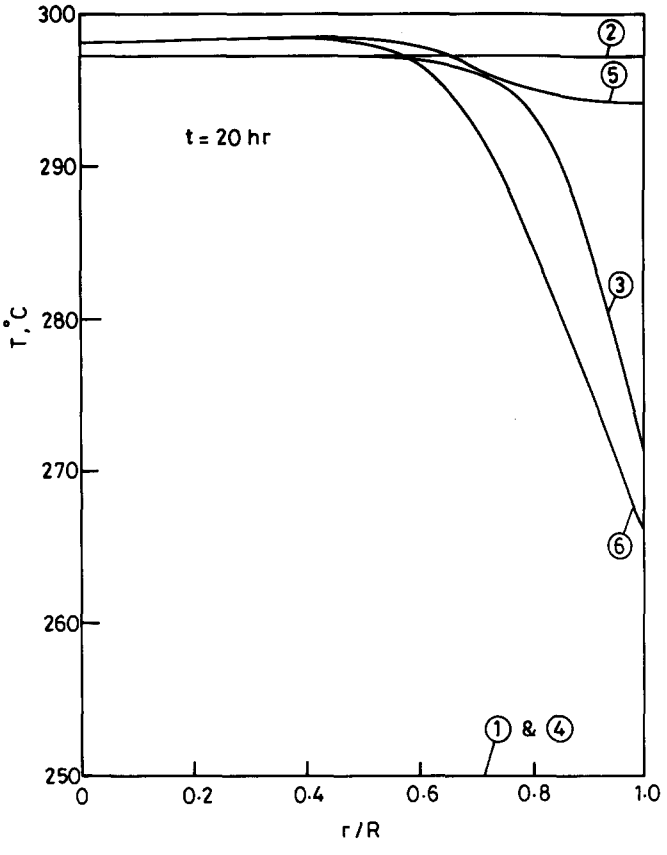

Figure 14 Radial profile for temperature at $t = 20$ h for various flow and heat transfer conditions (given in *Table 6*). Feed condition is as per equation (18)

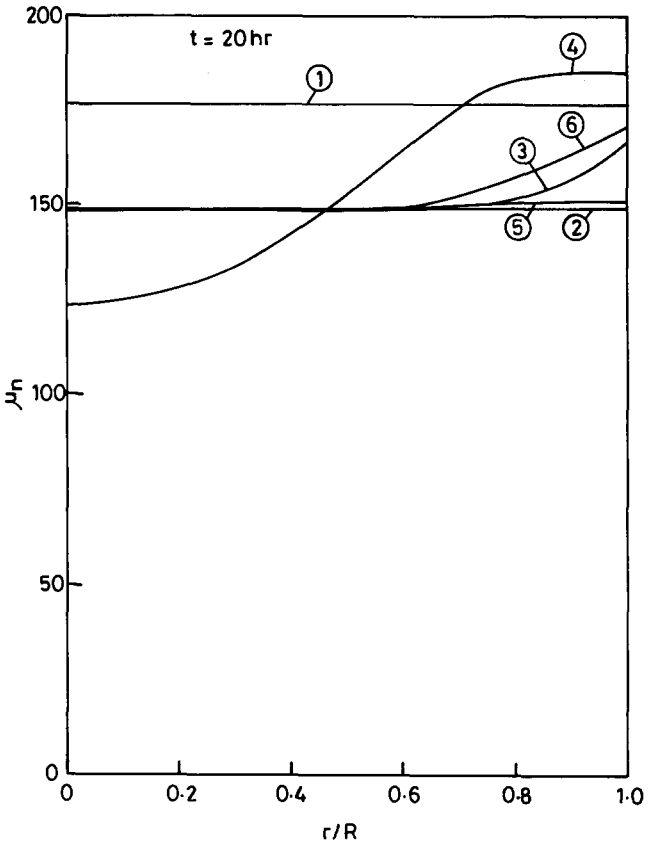

Figure 16 Radial profile for μ_n at $t = 20$ h. Conditions as in *Figure 14*

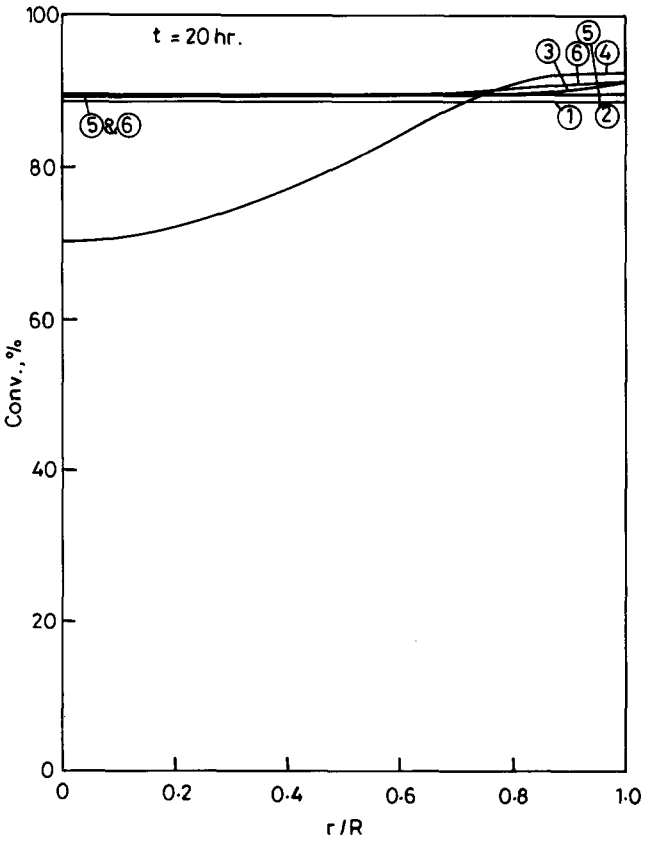

Figure 15 Radial profile for conversion at $t = 20$ h. Conditions as in *Figure 14*

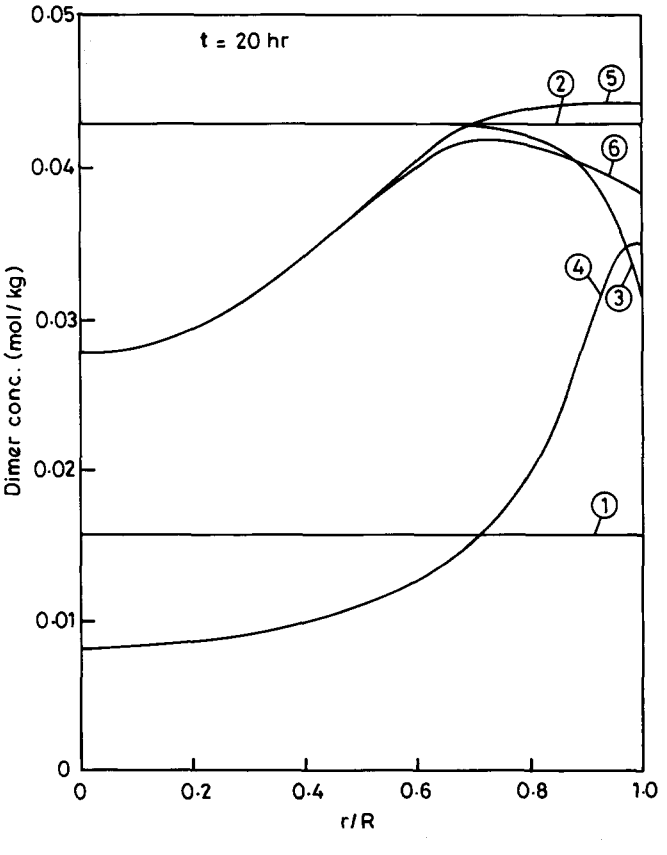

Figure 17 Radial profile for $[C_2]$ at $t = 20$ h. Conditions as in *Figure 14*

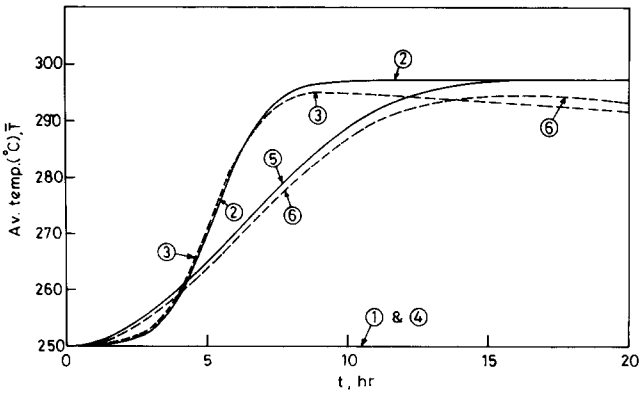

Figure 18 Axial variation of $\bar{T}$ for various flow and heat transfer conditions (given in *Table 6*) with feed condition as per equation (18)

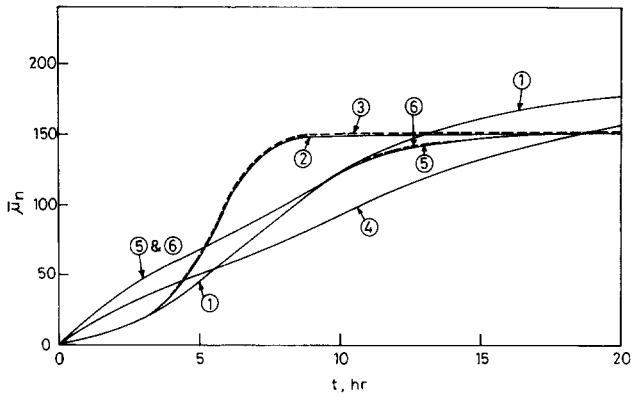

Figure 19 Axial variation of $\bar{\mu}_n$ for various flow and heat transfer conditions (given in *Table 6*) with feed condition as per equation (18)

This is because equilibrium for the cyclic dimer reactions has not yet been attained.

Figures 18 and *19* show the profiles of average temperature, $\bar{T}$, and average chain length, $\bar{\mu}_n$, along the reactor length for the various flow and heat transfer conditions of *Table 6*. It is interesting to note that the distinct *S* shape for the plug flow case (curves 2 and 3 in *Figure 18*) is relatively less prominent in the laminar flow case (curves 4 and 5 in *Figure 18*). Average temperatures for the non-adiabatic case (curves 3 and 6 in *Figure 18*) are in general lower than that for the adiabatic case (curves 2 and 3 in *Figure 18*) because of the cooling effects of the jacket fluid, except for the initial part of the plug flow case (curves 2 and 3 in *Figure 18*) where the jacket fluid has a heating effect as discussed earlier. For $\bar{\mu}_n$, again, the S shape in the case of plug flow (curves 1, 2 and 3 in *Figure 19*) is less prominent in laminar flow (curves 4, 5 and 6 in *Figure 19*). In general, isothermal operation (curves 1 and 4 in *Figure 19*) gives lower $\bar{\mu}_n$ in the initial part of the reactor because of comparatively lower temperatures in this case. But as t increases and equilibrium conversions are attained, $\bar{\mu}_n$ for the isothermal case registers higher values. It is observed that even though the $\bar{\mu}_n$ vs. t curves for adiabatic and non-adiabatic operation are almost identical, the actual radial variations of μ_n at any t are different in the two cases.

Table 7 shows the effects of the various parameters, e.g. radius of the reactor (R), coolant temperature (T_j), feed temperature (T_0) and feed water concentration ($[W]_0$), on the average values of temperature, monomer conversion, μ_n and cyclic dimer concentration. Decreasing the value of R to 0.4 m (run 2) from the reference conditions (run 1) helps to increase radial heat transfer since the area-to-volume ratio increases. Thus, the initial heating effects of the jacket fluid increases $\bar{T}$ at 5 h over that for the reference run. As t increases, the temperature is comparatively lower due to better cooling. However, average conversion and $\bar{\mu}_n$ are always lower. Increasing the value of R (run 3 on *Table 7*) has the opposite effect. A lower coolant temperature (run 4 in *Table 7*) causes lower temperatures in the reactor. This reduces the average conversion and $\bar{\mu}_n$ initially. But, as equilibrium is attained at higher values of t, the average conversion and $\bar{\mu}_n$ are higher as an effect of lower temperatures. A lower feed temperature (run 5 in *Table 7*) causes lower $\bar{T}$. As before, the average conversion and $\bar{\mu}_n$ are initially lower, but are higher near equilibrium. Lower feed water concentrations (run 6 in *Table 7*) cause lower conversions and $\bar{\mu}_n$ initially, as the ring-opening step (step 1 in *Table 1*) is slower. But as t increases, and near-equilibrium conditions are attained, monomer conversion improves and reaches the values for the reference state, since equilibrium conversion of the polycondensation reaction (step 2 in *Table 1*) is higher for lower [W]. The effect on $\bar{\mu}_n$ is much more pronounced. This is because a shift in the equilibrium for the polycondensation step to the right-hand side increases the chain length considerably. The effects of higher initial water concentration (run 7 in *Table 7*) are opposite in comparison to run 6 in *Table 7*.

The effect of some 'computational' variables is now studied. The value of the 'slip', i.e. the non-dimensional velocity ($v_z(R)/v_{av}$) assumed at the wall (to avoid numerical overflow and other computational problems), was changed around the reference value of 10^{-4} and some typical results are shown in *Table 8*. It is observed that the results are relatively unaffected by changing the slip, but the CPU time requirement increases for lower values of the slip. Similarly, instead of using the actual feed conditions at $t=0$, $r=R$, values of $[C_1]_0$, $[W]_0$, $[P_1]_0$, etc., close to equilibrium values at the wall temperature were used for the laminar flow case, to make the equations less stiff. These values were changed to see their effect on the numerical results further down the reactor. The results were found to be quite insensitive to this change, but feeding in the near-equilibrium values reduced the computational time.

Figure 20 shows the effect of increasing the number of FD grid points (non-equispaced) on the results at $t=5$ h. The runs were made using method III, with the spacing of grid points denser near the wall (equation (15)). The figure shows very clearly that the results, particularly near the wall, converge as the number of points is increased and after about eight points the results do not show any major discrepancy. The results for more than 10 points are almost indistinguishable from those for 10 points.

Methods I and III (with the latter program run for identical placement of equispaced FD grid points) were found to give the same results for various reactor conditions. This confirms that these two computer programs, one in the NAG Library and one made by us, are almost the same. Both of them use the FD technique with Gear's method. Method III, however, is more flexible since it permits the use of unequal spacing of FD grid points, and is highly recommended.

Some discrepancy near the wall was found between

Table 7 Effect of various parameters on average values

Run	Description[a]	t (h)	$\bar{T}$ (°C)	Avg. conv. (%)	$\bar{\mu}_n$	$[\bar{C}_2]$
1.	*Reference conditions*:	5	264.09	28.24	67.08	0.00516
	Laminar flow	10	287.20	73.66	123.83	0.01788
	Non-adiabatic ($h=5$)	15	294.09	88.50	149.61	0.03003
	$R=0.6$ m	20	293.83	89.65	151.36	0.03702
	$T_j=260$°C					
	$T_0=250$°C					
	Feed condition as per equation (18)					
2.	$R=0.4$ m	5	264.27	29.09	68.79	0.00497
		10	287.06	74.89	126.46	0.01782
		15	292.90	88.80	150.72	0.03002
		20	292.01	89.78	152.52	0.03684
3.	$R=0.8$ m	5	263.96	27.66	65.69	0.00524
		10	287.39	73.19	122.80	0.01786
		15	294.71	88.38	149.09	0.03000
		20	294.73	89.59	150.80	0.03706
4.	$T_j=250$°C	5	263.49	28.03	66.71	0.00486
		10	286.44	73.67	124.19	0.01751
		15	293.12	88.55	150.22	0.02969
		20	292.64	89.73	152.13	0.03670
5.	$T_0=240$°C	5	247.96	15.38	53.06	0.00253
		10	264.57	47.73	89.55	0.00940
		15	278.46	74.90	128.58	0.01757
		20	284.75	88.09	153.77	0.02685
6.	$[W]_0=0.13$ mol kg^{-1}	5	260.25	20.76	65.07	0.00352
		10	280.21	60.04	117.87	0.01301
		15	292.05	84.16	161.87	0.02413
		20	293.84	89.17	170.77	0.03260
7.	$[W]_0=0.18$ mol kg^{-1}	5	266.66	33.24	67.38	0.00638
		10	290.52	80.16	125.50	0.02108
		15	294.38	89.30	140.50	0.03305
		20	293.72	89.71	141.25	0.03892
8.	$h=10$ kcal m^{-2} K^{-1} h^{-1}	5	263.88	28.22	67.07	0.00508
		10	286.89	73.67	123.99	0.01775
		15	293.70	88.52	149.86	0.02991
		20	293.38	89.68	151.65	0.03690

[a] All other values in runs 2–8 are as in reference conditions

Table 8 Effect of slip on simulation runs

Run[a]	Slip used	Wall temp. at 5 h (°C)	CPU time (for $t=5$ h)
1	10^{-4} (ref)	287.51	2 min 25 s
2	10^{-6}	287.51	3 min 5 s
3	10^{-3}	287.51	2 min 6 s

[a] All runs are for laminar flow adiabatic reactor with feed condition as per equation (18)

Table 9 Comparison of methods I and II[a] (laminar flow adiabatic reactor)

No. of FD points, $(N+1)$	Temp. at the wall (T_{N+1}) at $t=5$ h (°C)	
	Method I	Method II
9	290.04	294.85
12	285.72	288.68
15	287.62	288.04
20	287.50	287.50

[a] Equispaced grid points

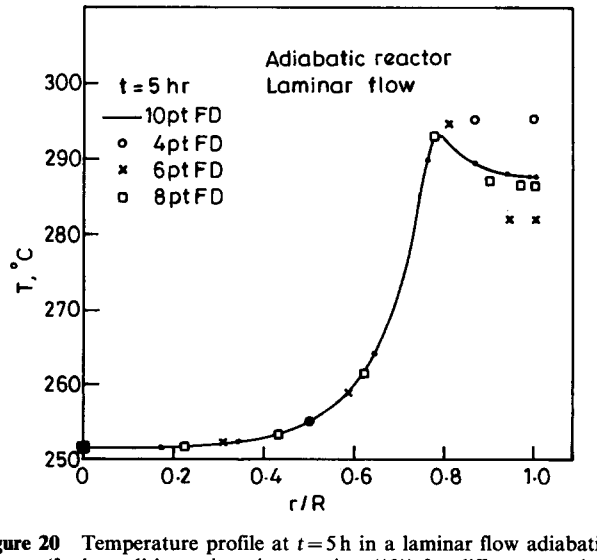

Figure 20 Temperature profile at $t=5$ h in a laminar flow adiabatic reactor (feed conditions given in equation (18)) for different number of non-equispaced grid points using finite difference (method III)

the results obtained using methods I and II. It may be mentioned that these two FD techniques differ only in terms of the boundary conditions. *Table 9* shows the wall temperatures (which are most sensitive) for the laminar flow adiabatic reactor as predicted by methods I and II, at $t=5$ h. With nine FD grid points the results show some differences at the wall, though those at the internal positions agree well. The reason for this discrepancy lies in the fact that, in method II, the wall temperature is obtained using the boundary condition alone (equation (14)). Therefore, the ODE from the heat balance equation at the wall ($r=R$), and thus the heat-of-reaction information near that location, is not used. In method I, on the other hand, both the boundary condition and the ODE from the heat balance are used at $r=R$. Therefore, when the gradients are steep near the wall (for lower values of t), method I gives better predictions. Thus, method I is superior to method II, particularly with regard to the results near the wall. However, as the number of FD points is increased, the results for both the methods should and do indeed converge as seen in *Table 9*. Similar results are obtained for the non-adiabatic case. However, for the non-adiabatic case of the plug flow reactor, where the temperature gradients near the wall are not so steep, the results agree well for the two methods (I and II).

CONCLUSIONS

A comprehensive study of the simulation of nylon-6 polymerization in a non-vaporizing continuous-flow tubular reactor was presented, taking into consideration the radial temperature and hence concentration variations arising out of radial thermal diffusion and laminar flow profile. A very general computer package was prepared to solve the set of differential equations obtained from the mass and heat balances, for isothermal, adiabatic and non-adiabatic operations and for both the cases of plus flow and laminar flow profiles. Two types of finite-difference methods (methods I and II) were used to convert the PFDs into ODEs, which were subsequently solved using Gear's method. Another program (method III) from the NAG Library, which uses a combined package of finite difference and Gear's method and uses non-equispaced grid points and so is more powerful, was also used.

A comparison of the various methods was made. Methods I and III were found to be essentially similar, with the latter having more flexibility as it could use any type of spacing of grid points. Method II was found to give poorer results near the wall, particularly when the temperature gradient near the wall was steep. Both methods I and II, however, agreed well as the number of grid points was increased.

REFERENCES

1 Reimschuessel, H. K. *J. Appl. Polym. Sci, Macromol. Rev.* 1977, **12**, 65
2 Tai, K. and Tagawa, T. *Ind. Eng. Chem., Prod. Res. Dev.* 1983, **22**, 192
3 Kumar, A. and Gupta, S. K. *J. Macromol. Sci., Rev. Macromol. Chem. Phys. (C)* 1986, **26**, 183
4 Gupta, S. K. in 'Encyclopedia of Engineering Materials', Vol. I, 'Properties and Synthesis' (Ed. N. P. Cheremisinoff), Dekker, New York, 1988
5 Gupta, S. K. and Kumar, A. 'Reaction Engineering of Step Growth Polymerization', Plenum, New York, 1987
6 Tai, K., Teranishi, H., Arai, Y. and Tagawa, T. *J. Appl. Polym. Sci.* 1980, **25**, 77
7 Tai, K., Arai, Y. and Tagawa, T. *J. Appl. Polym. Sci.* 1982, **27**, 731
8 Nagasubramanian, K. and Reimschuessel, H. K. *J. Appl. Polym. Sci.* 1972, **16**, 929
9 Mochizuki, S. and Ito, N. *Chem. Eng. Sci.* 1978, **33**, 140
10 Gupta, A. and Gandhi, K. S. 'Frontiers in Chemical Reaction Engineering' (Eds. L. K. Doraiswamy and R. A. Mashelkar), Wiley Eastern, New Delhi, 1984, pp. 667–82.
11 Gupta, S. K. and Tjahjadi, M. *J. Appl. Polym. Sci.* 1987, **33**, 933
12 Gupta, A., Gupta, S. K., Gandhi, K. S., Ankleswaria, B. V., Mehta, M. H., Padh, M. R. and Soni, A. V. 'Recent Trends in Chemical Reaction Engineering' (Eds. B. D. Kulkarni, R. A. Mashelkar and M. M. Sharma), Wiley Eastern, New Delhi, 1987, pp. 281–97
13 Naudin ten Cate, W. F. H. 'Proc. Int. Congr. on Use of Electronic Computers in Chemical Engineering', Paris, April 1973
14 Nagasubramanian, K. and Reimschuessel, H. K. *J. Appl. Polym. Sci.* 1973, **17**, 1663
15 Tai, K., Arai, Y. and Tagawa, T. *J. Appl. Polym. Sci.* 1983, **28**, 2727
16 Tai, K. and Tagawa, T. *J. Appl. Polym. Sci.* 1982, **27**, 2791
17 Gupta, S. K., Kumar, A., Tandon, P. and Naik, C. D. *Polymer* 1981, **22**, 481
18 Gupta, S. K., Naik, C. D., Tandon, P. and Kumar, A. *J. Appl. Polym. Sci.* 1981, **26**, 2153
19 Kumar, A. and Gupta, S. K. *Polymer* 1981, **22**, 1760
20 Hamer, J. W. and Ray, W. H. *Chem. Eng. Sci.* 1986, **41**, 3083
21 Jacobs, H. and Schweigman, C. 'Proc. 5th Eur./2nd Intl. Symp. on Chemical Reaction Engineering', Amsterdam, 2–4 May, 1972, p. B7.1
22 Arai, Y., Tai, K., Teranishi, H. and Tagawa, T. *Polymer* 1981, **22**, 273
23 Finlayson, B. A. 'Nonlinear analysis in Chemical Engineering', McGraw-Hill, New York, 1980
24 Gill, P. E. and Miller, G. F. *Comput. J.* 1972, **15**, 80
25 Ray, A. K. and Gupta, S. K. *Polymer* 1986, **26**, 1033

NOMENCLATURE

A_i^o, A_i^c	Frequency factors
C_1	ε-caprolactam
C_2	Cyclic dimer
C_p	Specific heat (kcal kg^{-1} K^{-1})
$(C_p)_j$	Specific heat at the jth grid point (kcal kg^{-1} K^{-1})
E_i^o, E_i^c	Activation energy
h	Overall heat transfer coefficient (kcal m^{-2} K^{-1} h^{-1})
ΔH_i	Enthalpy of reaction (cal mol^{-1})
k	Thermal conductivity (kcal m^{-1} K^{-1} h^{-1})
k_i	Forward rate constant
k_i'	Backward rate constant
K_i	Equilibrium constant
N	Number of internal grid points (excluding the point at the wall)
P_1	Aminocaproic acid
P_n	Polymeric species of chain length n
ΔQ	Overall heat of generation (kcal kg^{-1} h^{-1})
r	Radius (m)
r_j	Radial distance of jth grid point (m)
Δr	Distance between two grid points in finite difference (equal spacing) (m)
R	Reactor radius (m)
R_g	Universal gas constant (cal mol^{-1} K^{-1})
ΔS_i	Entropy of reaction (eu)
t	Average residence time (h)
T	Temperature (K)
$\bar{T}$	Average temperature at any cross-section (K)
T_j	Coolant temperature in jacket (K)

$U_{i,j}$	ith variable at jth grid point
v_z	Axial velocity ($m\,h^{-1}$)
v_{av}	Average axial velocity ($m\,h^{-1}$)
W	Water
x	Non-dimensional radius
x_j	Non-dimensional radius at jth grid point
z	Axial distance (m)
λ_k	kth moment for the polymeric species ($mol\,kg^{-1}$)
ρ	Density ($kg\,m^{-3}$)
ρ_j	Density at jth grid point ($kg\,m^{-3}$)
μ_n	Number-average chain length
$\bar{\mu}_n$	Average value of the number-average chain length at any cross section

Subscript

0	Initial value in the feed

Symbol

[ ]	Concentration of a species ($mol\,kg^{-1}$)